Extension of the Fenske−Hall Molecular Orbital Approach to Tight-Binding Band Structure Calculations: Bulk and Surface Electronic Structure of MoS_2

Agnes Tan[‡] and Suzanne Harris*

Department of Chemistry, University of Wyoming, Laramie, Wyoming 82071

Received July 11, 1997

A new tight-binding band structure calculation method is described. This method, which is based on the Fenske−Hall molecular orbital technique, should be extremely useful in the study of the bulk and surface electronic structure of inorganic materials. The approximations used in the Fenske−Hall method are reviewed, and the extension of this approach to periodic band structure calculations is outlined. Results of calculations for bulk MoS_2 are in good agreement with previous experimental and theoretical results. Results of calculations for two-dimensional MoS_2 slabs exposing (100) edge planes provide a description of coordinatively unsaturated Mo and S atoms on these edges. Coordinative unsaturation at the Mo atoms introduces new surface states near the Fermi level. Coordinative unsaturation at the S atoms leads to high-energy occupied bands that can be attributed to S lone pair electrons. Surface bonds between Mo atoms and terminal S atoms are stronger than bulk Mo−S bonds, suggesting that terminal S atoms may be more difficult to remove from the edges of MoS_2 than bridging S atoms. Bonding in a single two-dimensional layer of MoS_2 is found to be more ionic than the bonding in the full three-dimensional structure. This effect is also observed in one-dimensional MoS_2 ribbons that expose (100) edge planes. The simplified one-dimensional ribbons will be used for further studies of the electronic structure of the edge planes of MoS_2.

Introduction

In recent years, a number of computational techniques have been developed for studying the electronic structure of solids and surfaces. The algorithms are generally based on either first principles[1−4] or semiempirical methods.[5,6] First principles (ab initio) techniques are rigorous and potentially accurate, but they are invariably computationally intensive. Their application to solids which incorporate transition metals and have large unit cells is hampered by the sheer size of the calculation. Furthermore, even though such methods have the potential to provide accurate total energies, they may not provide a great deal of physical insight. Semiempirical methods (e.g. extended Hückel and CNDO), on the other hand, are considerably simpler; the choice of suitable parameters enables one to obtain meaningful qualitative results with a great reduction in computational effort. At the same time, however, a lack of self-consistency and/or the parametrization of the matrix elements often introduce(s) considerable uncertainty into both the calculated energies and charge distributions.

As a complement to these two classes of techniques, there is a place for a band structure algorithm incorporating a method intermediate in rigor. In the realm of molecular calculations, this place has long been occupied by the Fenske−Hall molecular orbital method.[7] The Fenske−Hall method is an approximate molecular orbital technique which utilizes a self-consistent field procedure. It is nonempirical, in that there is no parametrization of matrix elements, but the approximations invoked significantly reduce the amount of computation required. In other words, the Fenske−Hall approach is an approximation to a first-principles Hartree−Fock calculation. While total energies are not readily obtained from this method, the approach does yield a reliable description of the electron distributions and orbital energies for complex transition metal systems.

This report describes the extension of the Fenske−Hall molecular orbital method to a tight-binding band structure formalism for periodic systems. We are interested in the surface electronic structure of inorganic solids (such as transition metal sulfides and oxides) that serve as catalysts in heterogeneous processes, and this computational approach provides a new tool to study the electronic structure of such materials. This new Fenske−Hall band structure method will enable us to obtain reliable descriptions of the electron distributions and bonding in these often very complex solid state systems. In systems such as promoted transition metal sulfide hydrodesulfurization (HDS) catalysts, for example, a reliable description of the charge distributions and orbital structures of different possible active surfaces and catalytic sites would greatly further our understanding of the basis for the catalytic activity of these materials. The large unit cells required for studies of the surfaces of these materials mean, however, that ab initio calculations for these systems are usually limited to studies of very simplified models. Semiempirical techniques can easily treat large unit cells and provide a qualitative description of the bonding. They cannot, however, provide a reliable description of the charge distributions, possibly a critical factor in understanding what determines

[‡] Present Address: Institute of Molecular and Cell Biology, National University of Singapore, Kent Ridge, Singapore 119260.

(1) Pisani, C.; Dovesi, R.; Roetti, C. *Hartree−Fock Ab Initio Treatment of Crystalline Systems*; Springer-Verlag: Berlin, 1988.
(2) Schluter, M.; Chelikowsky, J. R.; Louie, S. G.; Cohen, M. L. *Phys. Rev. B* **1976**, *12*, 4200.
(3) Hedin, L.; Lundqvist, B. I. *J. Phys. C* **1971**, *4*, 2064.
(4) *Density Functional Methods: Application in Chemistry and Material Science*; Springborg, M., Ed.; Wiley: Chichester, UK, 1997.
(5) Whangbo, M.-H.; Evain, M.; Hughbanks, T.; Kertesz, M.; Wijeyesekera, S.; Wilker, C.; Zheng, C.; Hoffmann, R. *Extended Hückel Molecular, Crystal and Properties Package*; QCPE Program 571; Quantum Chemistry Program Exchange: Indiana University: Bloomington, IN.
(6) Craig, B. I.; Smith, P. V. *Phys. Stat. Sol. B* **1988**, *146*, 149.
(7) Hall, M. B.; Fenske, R. F. *Inorg. Chem.* **1972**, *11*, 768.

S0020-1669(97)00874-4 CCC: $15.00
Published on Web 04/08/1998

an active catalytic site. For these kinds of solid-state systems, the Fenske−Hall band structure technique will offer an approach that is intermediate in rigor but also yields chemically useful information.

The first section of the paper reviews the features of the Fenske−Hall molecular orbital approach and outlines the development and implementation of this approach for periodic band structure calculations. The second section discusses the results of bulk electronic structure calculations for MoS_2 and compares these results to prior work. MoS_2, which serves as a catalyst for the hydrodesulfurization (HDS) of the sulfur containing aromatic compounds found in petroleum feedstocks,[8] has been the subject of several experimental and theoretical investigations and therefore provides an ideal "test case" for the Fenske−Hall calculations. The third section describes the calculated electronic structure of (100) surface planes of MoS_2. Coordinatively unsaturated Mo atoms on these edge planes are believed to provide the active sites for HDS catalysis.[9] Finally, the last section discusses the effects of modeling MoS_2 with a single MoS_2 sheet. Use of this simplified system would enable us to study the electronic structure both of edge planes having isolated sulfur vacancies and of models for promoted MoS_2 catalysts while maintaining a reasonably small unit cell size.

Mathematical Formalism

Fenske−Hall Molecular Orbital Method. For clarity, we first review the key features of the Fenske−Hall molecular orbital method.[7] In this approach, electron density is assigned to each center in the system through Mulliken population analyses,[10] and a point charge approximation is invoked in the calculation of multicenter coulomb and exchange terms. These and other standard approximations form the basis for constructing the Hartree−Fock−Roothaan[11] (HFR) matrix. The diagonal matrix element for atomic orbital φ_a (on center A) is

$$F_{aa} = \epsilon_a - \sum_{C \neq A} \frac{q_C}{R_{AC}} \tag{1}$$

where ϵ_a is the atomic orbital energy of an electron in φ_a, in which the one-center interelectron repulsions are calculated using Slater's average of configuration approach;[12] q_C is the Mulliken charge on center C (nuclear charge less the sum of Mulliken populations); and R_{AC} is the distance between centers A and C. The energetic placement of φ_a is determined primarily by F_{aa}, and the value of F_{aa} depends on several factors. Two of these factors, the kinetic energy and nuclear attraction terms, do not depend on the charge distribution, but two other factors *do* vary with the charge distribution. First, interelectron repulsions due to the occupation of atomic orbitals on the same center destabilize F_{aa}; second, an environmental factor (also related to electron repulsion) destabilizes F_{aa} if neighboring atoms are negatively charged and stabilizes F_{aa} if these neighboring atoms are positively charged.

Two-center off-diagonal elements between atomic orbitals φ_a and φ_b (on centers A and B, respectively) are expressed as follows:

$$F_{ab} = \langle\varphi_a|\varphi_b\rangle(\epsilon_a + \epsilon_b) - \langle\varphi_a| - {}^1/_2\nabla^2|\varphi_b\rangle - {}^1/_2\langle\varphi_a|\varphi_b\rangle \sum_{C \neq A,B}\left(\frac{q_C}{R_{AC}} + \frac{q_C}{R_{BC}}\right) \tag{2}$$

The overlap and kinetic energy integrals, $\langle\varphi_a|\varphi_b\rangle$ and $\langle\varphi_a| - {}^1/_2\nabla^2|\varphi_b\rangle$, are evaluated exactly, while the other terms are evaluated as in eq 1. One-center off-diagonal elements are set to zero.

The HFR equation[11]

$$\mathbf{FC} = \mathbf{SC}\epsilon \tag{3}$$

($\mathbf{S}$ = overlap matrix; $\mathbf{C}$ = eigenvector matrix; ϵ = diagonal eigenvalue matrix) can then be solved by standard techniques. Since the $\mathbf{F}$ matrix depends on the $\mathbf{C}$ matrix through the Mulliken populations, this equation must be solved to self-consistency.

Extension to Periodic Systems. In general, a molecular orbital technique can be extended to periodic systems by recognizing the translational symmetry through the use of Bloch functions.

$$\Phi_a(\vec{k}) = \frac{1}{\sqrt{N}} \sum_{\tau} \varphi_a{}^{\tau} e^{i\vec{k}\cdot\vec{\tau}} \tag{4}$$

where N is the total number of unit cells in the system; $\vec{\tau}$ is the translation vector between two lattice points; $\vec{k}$ is a reciprocal lattice vector; and $\varphi_a{}^{\tau}$ refers to the basis function φ_a on center A in the unit cell at the vector distance $\vec{\tau}$ from the zeroth unit cell. The HFR and overlap matrixes can be constructed in analogy to the molecular case for a particular reciprocal lattice vector $\vec{k}$:

$$F_{ab}(\vec{k}) = \langle\Phi_a(\vec{k})|F|\Phi_b(\vec{k})\rangle = \sum_{\tau} F_{ab}{}^{\tau} e^{i\vec{k}\cdot\vec{\tau}}$$

$$S_{ab}(\vec{k}) = \sum_{\tau} S_{ab}{}^{\tau} e^{i\vec{k}\cdot\vec{\tau}} \tag{5}$$

In terms of the molecular case, $F_{ab}{}^{\tau} = \langle\varphi_a{}^{o}|F|\varphi_b{}^{\tau}\rangle$ is the matrix element between φ_a in the zeroth unit cell and φ_b in the unit cell at $\vec{\tau}$ and is modulated by the phase factor $e^{i\vec{k}\cdot\vec{\tau}}$. The $\mathbf{S}$ matrix is similarly defined. The energy of φ_a is $F_{aa}{}^{o}$, the equivalent of the molecular diagonal element, where the "o" refers to both functions being in the same (zeroth) unit cell. It should be noted that the phase factor can be written either as $e^{i\vec{k}\cdot\vec{\tau}}$, as in eq 5, or as $e^{i\vec{k}(\vec{\tau}+\vec{r}_B-\vec{r}_A)}$, where $\vec{r}_A$ and $\vec{r}_B$ are the positions of centers A and B in the unit cell. In either form the Bloch theorem is obeyed, and there is no difference numerically. We have adopted the notation shown in eq 5 in order to be consistent with our definition of the Bloch functions. Physically, this means that we are taking into account the periodicity of the entire unit cell.

If we return to the Fenske−Hall method, the terms $F_{ab}{}^{\tau}$ and $S_{ab}{}^{\tau}$ can be evaluated in analogy to the molecular case. That is

$$F_{aa}{}^{o} = \epsilon_a - \sum_{\tau}\sum_{C \neq A^o} \frac{q_C}{R_{AC}{}^{\tau}} \tag{6a}$$

where the sum over C includes A in all other unit cells except the zeroth and

$$F_{ab}{}^{\tau} = S_{ab}{}^{\tau}(\epsilon_a + \epsilon_b) - \langle\varphi_a{}^{o}| - {}^1/_2\nabla^2|\varphi_b{}^{\tau}\rangle - {}^1/_2 S_{ab}{}^{\tau} \sum_{\tau'}\sum_{C \neq A^o, B^{\tau}} \left(\frac{q_C}{R_{AC}{}^{\tau'}} + \frac{q_C}{R_{BC}{}^{\tau'-\tau}}\right) \tag{6b}$$

In eq 6a, the two-center electrostatic term

$$Q_A = -\sum_{\tau}\sum_{C \neq A^o} \frac{q_C}{R_{AC}{}^{\tau}}$$

is simply the negative of the electrostatic potential experienced by the atom A and can be calculated using the Ewald summation technique (see Appendix). The three-center terms that appear in $F_{ab}{}^{\tau}$ can be calculated from the Ewald sums by recognizing that

(8) Topsøe, T.; Clausen, B. S.; Massoth, F. E. *Hydrotreating Catalysis*; Springer-Verlag: Berlin, 1996.
(9) Chianelli, M.; Daage, M.; Ledoux, M. J. *Adv. Catal.* **1994**, *40*, 177.
(10) Mulliken, R. S. *J. Chem. Phys.* **1955**, *23*, 1833.
(11) Roothaan, C. C. J. *Rev. Mod. Phys.* **1951**, *23*, 69.
(12) Slater, J. C. In *Quantum Theory of Atomic Structure*; McGraw-Hill: New York, 1960; p 322.

$$-\sum_{\tau'}\sum_{C\neq A^o,B^r}\left(\frac{q_C}{R_{AC}{}^{\tau'}}+\frac{q_C}{R_{BC}{}^{\tau'-\tau}}\right)=Q_A+Q_B+\frac{q_A+q_B}{R_{AB}{}^{\tau}}$$

As before, the charges on the various atoms are obtained via Mulliken population analyses.

Since the matrices $\mathbf{F}(\vec{k})$ and $\mathbf{S}(\vec{k})$ are both Hermitian, the corresponding HFR equation

$$\mathbf{F}(\vec{k})\mathbf{C}(\vec{k})=\mathbf{S}(\vec{k})\mathbf{C}(\vec{k})\epsilon(\vec{k}) \qquad (8)$$

can be solved to yield real eigenvalues. The vector $\vec{k}$ can take on any real value within the first Brillouin zone, constituting a continuous distribution. For example, for an orthorhombic (i.e. with all faces rectangular) unit cell, the first Brillouin zone is defined by $0 \leq k_x, k_y, k_z \leq \pi/a, \pi/b, \pi/c$, where *a*, *b*, and *c* are the dimensions of the unit cell. In practice, however, finite *k* point sets are used, and these may be tailored to the symmetry of the system. Procedures for *k* point sampling are documented elsewhere.[13−16]

In the calculation of properties such as the density of states, atomic and fragment molecular orbital populations, overlap populations, and crystal orbital overlap population (COOP) curves, the computational approach we have adopted is similar to that used in the extended Hückel program of Whangbo and co-workers.[5]

Calculational Details for MoS_2. Calculations on bulk MoS_2 are based on the known crystal structure of the solid.[17] Surface calculations for MoS_2 were carried out on unreconstructed surfaces. The *k* points were sampled from the irreducible Brillouin zone (IBZ) of the appropriate Patterson space groups, as documented by Ramírez and Böhm;[13,14] these are listed in Table 1.

Atomic basis functions were obtained by fitting the results of Xα (Herman−Skillman) calculations[18] for a given atomic charge to Slater type orbitals.[19] In molecular Fenske−Hall calculations transition metal basis functions are generally chosen by calculating a modified Mulliken charge for the metal which is based on the d orbital populations only; this modified charge, rounded to the nearest integer, determines the choice of the 1s through valence d orbital functions. It became clear while testing the program that this procedure is unsuitable for selecting transition metal basis functions for the band structure calculations, since the valence d functions thus obtained, particularly for second-row transition metals, are too diffuse and lead to bandwidths that are too wide. As a result, transition metal 1s through valence d orbital basis functions used in the band structure calculations have been chosen by fitting the width of part or all of the d band to the width obtained from ab initio calculations on compounds of interest; when such calculations are unavailable, extrapolations from similar compounds are made. For second (and third) row transition metals, the basis functions need to be more contracted; this is less the case for the smaller first row transition metals. The calculated modified charge for Mo in MoS_2, for example, is +1.63, which in molecular calculations would dictate the use of functions corresponding to Mo^{2+}. To reproduce the d bandwidths, however, the results reported here used atomic basis functions corresponding to $Mo^{2.4+}$. As in molecular calculations, the Mo 5s and 5p functions were both chosen to have exponents of 2.2. The selection of basis functions for sulfur was more straightforward. Basis functions used in the calculations correspond to *S*(0). These functions are the usual choice in molecular calculations for sulfur atoms having a −2 oxidation state, and these same functions provide a reasonable fit to the sulfur p bandwidths in band structure calculations on transition metal sulfides.

(13) Ramírez, R.; Böhm, M. C. *Int. J. Quantum Chem.* **1986**, *30*, 391.
(14) Ramírez, R.; Böhm, M. C. *Int. J. Quantum Chem.* **1988**, *34*, 571.
(15) Monkhorst, H. J.; Pack, J. D. *Phys. Rev. B* **1976**, *13*, 5188.
(16) Pack, J. D.; Monkhorst, H. J. *Phys. Rev. B* **1977**, *16*, 1748.
(17) Wyckoff, R. W. G. In *Crystal Structures*; Wiley-Interscience: New York, 1963; p 280.
(18) Herman, F.; Skillman, S. *Atomic Structure Calculations*; Prentice Hall: Englewood Cliffs, NJ, 1963.
(19) Bursten, B. E.; Jensen, R. J.; Fenske, R. F. *J. Chem. Phys.* **1978**, *68*, 3320.

Table 1. Irreducible Brilloiun Zones (IBZ) and Number of *k* Points Used in MoS_2 Calculations

	IBZ	no. of *k* points
solids		
bulk MoS_2[a]	*P*6/*mmm*	216
MoS_2 sheet	2-D hexagonal	127
surfaces		
MoS_2 (100)	rectangular	100
MoS_2 (100) ribbon	1-D	100

[a] All calculations were carried out on an SGI Indy R5000 workstation. The CPU time required to reach convergence and generate all necessary files for DOS and COOP curves for bulk MoS_2 was 59 min. The CPU time required can be considerably reduced by decreasing the number of *k* points, making educated guesses for initial orbital populations, and utilizing an extrapolaton routine to estimate starting populations for successive cycles.

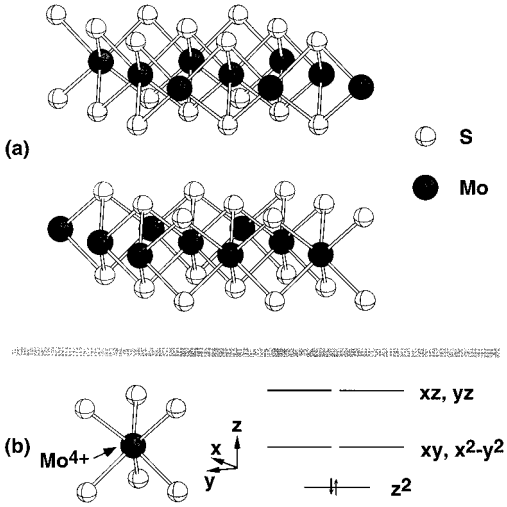

Figure 1. Structure of MoS_2. (a) Illustration of the stacking of small sections of MoS_2 sheets; (b) local trigonal prismatic coordination geometry of each Mo atom and corresponding crystal field splitting of the Mo 4d orbitals.

Results and Discussion

Electronic Structure of Bulk MoS_2. MoS_2 exhibits a layered structure composed of two-dimensional sheets which interact only through van der Waals forces (Figure 1a). The unit cell is hexagonal, and each molybdenum atom is surrounded by six sulfur atoms coordinated in a trigonal prismatic fashion (Figure 1b). The electronic structure of MoS_2 can be understood in terms of the ligand field orbital splitting expected for trigonal prismatic metals ($d_{z^2} < d_{x^2-y^2}$, $d_{xy} < d_{xz}$, d_{yz} for *z* along the vertical 3-fold axis of the trigonal prism), and this progression of metal bands is observed in the calculated total density of states (DOS) curve for MoS_2 shown in Figure 2a. Since each Mo is in the +4 oxidation state and formally has two 4d electrons, the d_{z^2} band is completely filled while the rest of the d bands are empty. The partial density of state curves, Figure 2b, reveals that there is some mixing between the d_{z^2} and the $d_{x^2-y^2}$, d_{xy} bands, indicating a measure of metal−metal interaction. This mixing was observed in the previous calculations of Yee and Hughbanks[20] and can be associated with metal−metal bonding involving orbitals in the *xy* plane. The semiconducting gap therefore separates what are nominally the d_{z^2} and ($d_{x^2-y^2}$, d_{xy}) bands. In fact, however, there is mixing between these sets of orbitals, and the gap separates groups of bands which are weakly Mo−Mo bonding and antibonding.

(20) Yee, K. A.; Hughbanks, T. *Inorg. Chem.* **1991**, *30*, 2321.

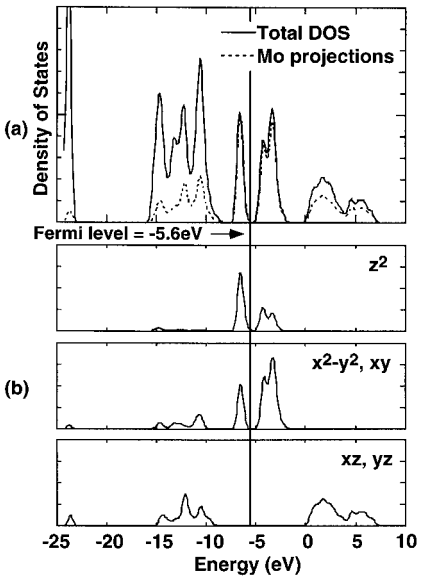

Figure 2. Calculated density of states (DOS) for bulk MoS_2. (a) Total DOS and Mo projections. The Mo projections include the total Mo orbital contribution to each band. (b) Individual Mo 4d orbital partial DOS.

The calculated bandwidths and character are in reasonable agreement with both photoelectron spectra and previous calculations on MoS_2.[20−23] (All of these previous calculations also showed a "d_{z^2}" band approximately 1 eV in width at the top of a 5−7 eV wide S 3p-derived band.) The size of the semiconducting gap was calculated to be 0.86 eV, which is within the range of reported experimental measurements. (Reported experimental values[24−26] range from 0.27 to 1.35 eV and include one at 0.8 eV.) An artifact of our calculations is the ∼1 eV gap between the sulfur p and molybdenum d_{z^2} bands; this gap is not observed in the photoelectron spectrum of MoS_2.[22] (It should be noted, however, that such a gap has also been found in previous calculations.) We have found such a gap (of varying width) to be present in all our calculations on second-row transition metal sulfides. This appears to result from approximations used in the Fenske−Hall method. Particularly, the use of point charge approximations tends to destabilize the metal orbitals, and the manner in which the off-diagonal elements F_{ab}^{τ} are calculated tends to exaggerate bonding−antibonding splittings). This means that if we wish to make comparisons between different sulfides we must recognize that our results overestimate the separation between the sulfur p and metal d bands. At the same time, however, the qualitative features of the band structures of MoS_2 and other transition metal sulfides[27] are modeled reasonably well, and comparisons may be readily made between bulk and surface calculations of the same compound.

MoS_2 (100) Surface(s). One of the main motivations for our development of a new band structure approach has been our interest in the surface electronic structure of inorganic solids that serve as catalysts in important chemical processes. Several transition metal sulfides show significant activity as HDS catalysts.[28] While it is generally accepted that active HDS sites on sulfides involve coordinatively unsaturated metal centers, there is little agreement as to exactly which metal site is active or how many sulfur vacancies exist in the metal coordination sphere at this active site. To try to answer these questions, we have begun a systematic study of the electronic structure of possible active surfaces on these sulfides.

We report here our first results for edge plane surfaces of MoS_2. MoS_2 itself shows significant activity as an HDS catalyst, and Co- or Ni-promoted MoS_2 is used in many industrial HDS processes. Although extended Hückel calculations have been used previously to study surfaces of MoS_2,[29] our results represent the first self-consistent study of these surfaces. In addition, these results provide a basis for further studies of surfaces consistent with the "CoMoS" and "NiMoS" models[30] of the promoted edge planes.

To study the electronic structures of surfaces it is necessary to carry out calculations on two-dimensional slabs of finite thickness. One or both of the surfaces of the slab then represents a surface of interest. Ideally, such a slab should be sufficiently thick that the internal atoms exhibit the electronic properties of "bulk" atoms. Since a slab has two- rather than three-dimensional translational symmetry, however, the size of the unit cell increases dramatically as the thickness of the slab increases. In reality some compromise between computational feasibility and a reasonable representation of the bulk solid must be made; we have generally chosen to use slabs which incorporate three or four layers of metal centers and their surrounding ligands.

Two MoS_2 surface planes of interest are the (001) basal plane and the (100) edge plane. A (001) basal plane is generated by slicing between two MoS_2 layers; this exposes a layer of triply bridging sulfur atoms. A (100) edge plane, on the other hand, is formed by slicing down through the layers to expose edges of the MoS_2 layers. It is generally accepted that the MoS_2 (001) basal plane shows little catalytic activity in the HDS process and that active sites occur on the edge plane (100) surface.[9] This edge plane is also associated with promotion by Co or Ni and the formation of the active "CoMoS" or "NiMoS" promoted catalytic phases.[8] We have thus begun our studies of the surfaces of metal sulfides by focusing on the (100) edge planes of MoS_2.

Slabs appropriate for studying the MoS_2 (100) edge can be constructed by cutting two planes (both parallel to the *xz* plane, in the coordinate system defined in Figure 3) through the bulk MoS_2 crystal. This generates surfaces that are periodic in the *x* and *z* directions. The edges of the MoS_2 layers repeat in the *x* direction, while the MoS_2 layers repeat in the *z* direction; the *y* dimension defines the thickness of the slab. The results presented here are based on slabs which are four Mo atoms thick; this limits the size of the unit cell and provides a reasonable description of the "bulk" atoms. The diagrams in Figure 3 show portions of slabs exposing the (100) edge. When all the edge Mo atoms are coordinatively saturated (Figure 3a), one surface of the slab exposes terminal sulfur atoms while the other exposes 2-coordinate bridging sulfur atoms. (Sulfur atoms in the bulk are 3-coordinate.) These are commonly referred to as the $(10\bar{1}0)$ and $(\bar{1}010)$ surfaces, respectively. While the slab shown in Figure 3a does not maintain the stoichiometry of MoS_2

(21) Mattheis, L. F. *Phys. Rev. Lett.* **1973**, *30*, 84.
(22) Wertheim, G. K.; DiSalvo, F. J.; Buchanan, D. N. E. *Solid State Commun.* **1973**, *13*, 1225.
(23) Coehoorn, R.; Haas, C.; Dijkstra, J.; Flipse, C. J. F.; de Groot, R. A.; Wold, A. *Phys. Rev. B* **1987**, *35*, 6195.
(24) Wilson, J. A.; Yoffe, A. D. *Adv. Phys.* **1969**, *18*, 193.
(25) Huisman, R.; de Jong, R.; Haas, C.; Jellinek, F. *J. Phys. C* **1971**, *10*, 1079.
(26) Yoffe, A. D. *Chem. Soc. Rev.* **1976**, *5*, 51.
(27) Tan, A.; Harris, S. *Inorg. Chem.* **1998**, *37*, 2215.
(28) Pecoraro, T. A.; Chianelli, R. R. *J. Catal.* **1981**, *67*, 430.
(29) Zonnevylle, M. C.; Hoffmann, R.; Harris, S. *Surf. Sci.* **1988**, *199*, 320.
(30) Topsøe, H.; Clausen, B. S.; Candia, R.; Wivel, C.; Mørup, S. *J. Catal.* **1981**, *68*, 433.

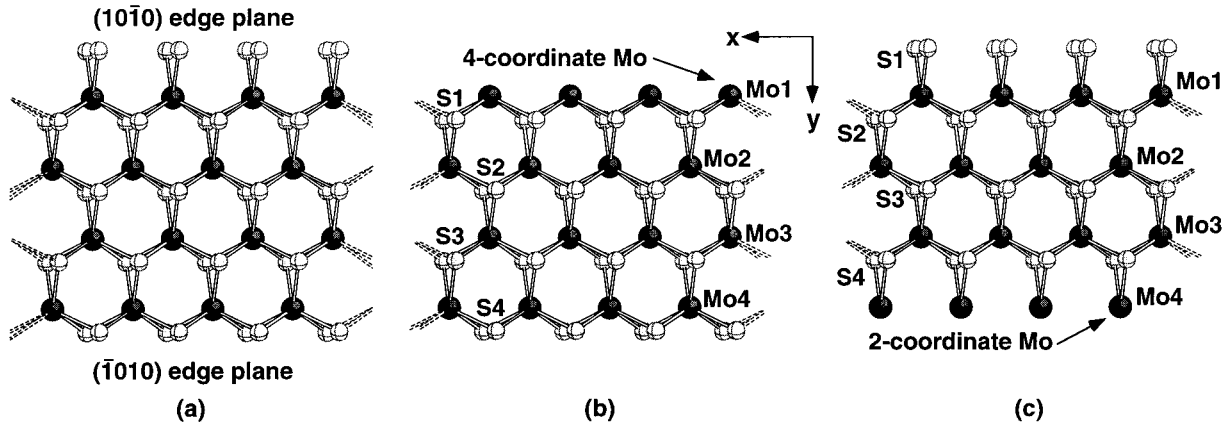

Figure 3. Portions of MoS_2 slabs exposing (10$\bar{1}$0) and ($\bar{1}$010) edge planes. Surfaces of the slabs are periodic in the *x* and *z* directions. Edges of the MoS_2 layers repeat in the *x* direction, and MoS_2 layers repeat in the *z* direction. (a) Slab exposing fully sulfided edges; (b) slab exposing 4-coordinate Mo atoms; (c) slab exposing 2-coordinate Mo atoms. (For calculations based on a single MoS_2 layer, (a−c) illustrate the one-dimensional ribbons exposing the edge planes.)

(there are excess sulfur atoms), the slabs actually used in the calculations (Figures 3b and 3c) do maintain the MoS_2 stoichiometry. In the first case (Figure 3b), the terminal sulfur atoms are removed from the (10$\bar{1}$0) edge plane of each MoS_2 layer. This exposes 4-coordinate Mo atoms on one surface of each MoS_2 layer but leaves the opposite side of the layer terminated by doubly bridging sulfurs; this will be referred to as the 4-coordinate slab. In the second case (Figure 3c), the bridging sulfur atoms are removed from the ($\bar{1}$010) edge plane of each MoS_2 layer. This exposes 2-coordinate Mo atoms on one surface of each layer but leaves the opposite side of the layer terminated by terminal sulfurs; this will be termed the 2-coordinate slab. Because the MoS_2 layers in bulk MoS_2 stack in an ...ABABABAB... pattern the S atom vacancies on the slabs alternate between the "top" and "bottom" sides of adjacent MoS_2 layers. For example, Figure 3b shows the sulfur vacancies occurring on the $-y$ side of the layer; the sulfur vacancies on the layers on either side of this layer (in the $+z$ or $-z$ direction) will occur on the $+y$ side of the slab. This same alternation occurs for the slab in Figure 3c.

Although it is unlikely that all of the terminal or bridging sulfurs would be removed from a MoS_2 edge, this first set of calculations provides a description of the orbital structure and charge distribution of 4-coordinate and 2-coordinate surface Mo atoms. At the same time, the opposite surface of each slab provides a description of a fully sulfided (1$\bar{0}$10) or ($\bar{1}$010) edge. Future calculations will consider more isolated vacancy patterns (at the expense of much larger unit cells and longer computation times).

Surface States of the 4-Coordinate Slab. Both surfaces of this slab expose coordinatively unsaturated atoms, 4-coordinate Mo centers (Mo1 in Figure 3b) on one surface, and 2-coordinate S centers (S4 in Figure 3b) on the other. The total DOS curve for the slab (Figure 4a) thus exhibits a number of surface states not found in the DOS of bulk MoS_2, and the semiconducting gap observed in the total DOS curve for bulk MoS_2 (Figure 2a) is absent in the slab. The projections of the surface Mo1 d orbitals and the projection of the bridging 2-coordinate S4 3s and 3p orbitals are also shown in Figure 4b and 4c, respectively. Comparisons between the Mo d orbital projections in bulk MoS_2 (Figure 2b) and the surface Mo d orbital projections in the slab (Figure 4b) show that the new surface states primarily arise from two sources. The largest effects stem from the loss of two nearest-neighbor S atoms. While all the surface Mo d bands are affected to some degree by this change in coordination

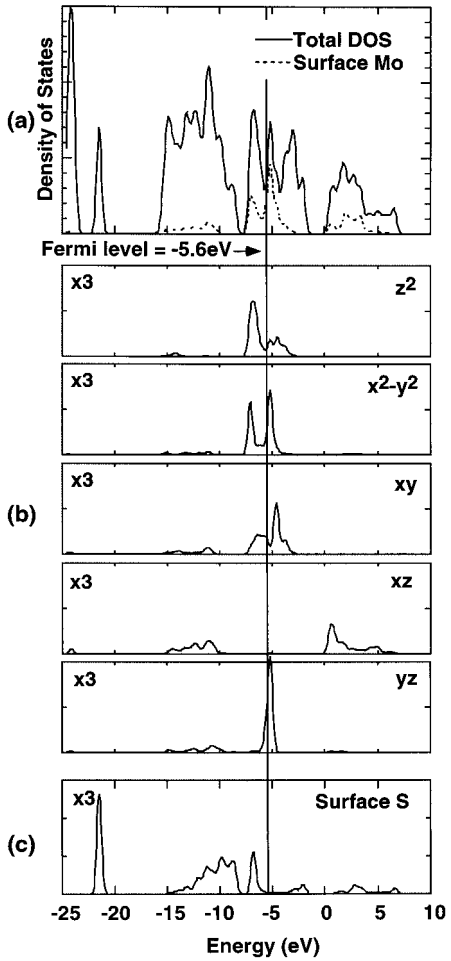

Figure 4. Calculated DOS for the MoS_2 slab exposing 4-coordinate Mo atoms. (a) Total DOS and projection of surface Mo (Mo1 in Figure 3b) orbitals. (b) Individual Mo1 4d orbital partial DOS. (c) Projection of surface S (S4 in Figure 3b) 3s and 3p orbital partial DOS.

geometry, the most noticeable change is the significant drop in energy of the surface Mo d_{yz} band; this results from the loss of σ interactions between this orbital and the two missing sulfur ligands. The d_{yz} band is thus stabilized and actually partially occupied. Effects on the other d orbitals are much smaller and appear to decrease in the order $d_{x^2-y^2} > (d_{z^2}, d_{xy}, d_{xz})$. At the same time, since the surface Mo atoms have two fewer next nearest-neighbor Mo atoms than the Mo atoms in the bulk, Mo−

Table 2. Calculated Mulliken Charges (q_A), Energy Levels ($F_{aa}{}^o$, EV, for Metal d and Sulfur p Orbitals), Potential Energies ($-Q_A$, eV), and Selected Mo−S Overlap Populations for Bulk MoS_2 and for the 4- and 2-Coordinate (100) Surface Slabs

	q_A	$F_{aa}{}^o$	$-Q_A$
	Bulk MoS_2		
Mo	1.05	−6.64	−7.34
S	−0.53	−11.12	5.68
	Mo−S overlap population 0.081		
	4-Coordinate Slab		
Mo1[a]	1.00	−6.76	−5.83
Mo2	1.15	−6.96	−8.21
Mo3	1.09	−6.50	−7.88
Mo4	1.33	−6.27	−11.55
S1	−0.56	−11.69	6.60
S2	−0.50	−11.54	5.84
S3	−0.55	−11.27	6.11
S4[a]	−0.68	−8.88	5.18
	Mo1−S1 overlap population 0.058		
	Mo4−S4 overlap population 0.084		
	2-Coordinate Slab		
Mo1	1.23	−6.60	−9.86
Mo2	1.08	−6.40	−7.82
Mo3	1.16	−6.50	−8.83
Mo4[a]	0.74	−5.69	−2.87
S1[a]	−0.44	−8.50	2.13
S2	−0.55	−11.36	6.17
S3	−0.53	−11.25	5.82
S4	−0.59	−11.22	6.48
	Mo1−S1 overlap population 0.120		
	Mo4−S4 overlap population 0.101		

[a] Surface atoms as defined in Figure 3.

Mo interactions involving surface Mo orbitals having components in the *xy* plane (d_{z^2}, $d_{x^2-y^2}$, and d_{xy}) are decreased, and the gap separating the bonding and antibonding combinations of these orbitals decreases. As a result, all of the surface Mo d orbitals except d_{xz} contribute to bands near the Fermi level.

Not surprisingly, the projection of the 3s and 3p orbitals of the doubly bridging S atoms which terminate the opposite side of the slab (Figure 4c) shows that both the s and p bands are destabilized relative to the corresponding bands in bulk MoS_2 (and to the "bulk" S atoms in the slab). The fairly narrow band (−7 to −6 eV) just below the Fermi level results from the coordinative unsaturation of the doubly bridging surface S atoms and can be associated with nonbonding S lone pair electrons.

Calculated Mulliken charges, diagonal terms of the Hartree−Fock matrix ($F_{aa}{}^\circ$) for the Mo 4d and S 3p orbitals, and electrostatic potentials ($-Q_A$) for Mo and S atoms in bulk MoS_2 and for all nonequivalent Mo and S atoms in the 4-coordinate slab are listed in Table 2. Comparisons between these values for the "bulk" atoms in the slab (Mo2, Mo3, S2, and S3) and for the Mo and S atoms in bulk MoS_2 show that the bulk is fairly well represented in the slab. While the 4-coordinate surface Mo atoms and the doubly bridging surface S atoms are both slightly reduced in comparison to bulk Mo and S atoms, the reduction of the S centers is greater. The diagonal matrix elements ($F_{aa}{}^o$) provide a measure of the Mo 4d and S 3p orbital energies of the surface atoms relative to those in the bulk, and it is clear that the levels of the doubly bridging S atoms are destabilized. In terms of the discussion concerning eq 1 and thus eq 6a, the destabilization of the surface S levels is caused partly by the increased negative charge and partly by the absence of the stabilizing effect of one positive nearest-neighbor Mo center. Although the surface Mo atoms are also slightly reduced, the d levels are not destabilized since any destabilization resulting from an increased orbital occupation is offset by the stabilizing effect of the loss of two negative nearest-neighbor S centers. Overlap populations involving surface Mo and S centers are also listed in Table 2. Comparison with the Mo−S overlap population in bulk MoS_2 provides a measure of the relative Mo−S bond strengths on the surfaces. While the remaining Mo−S bonds for the coordinatively unsaturated Mo centers are actually slightly weaker than in the bulk, the Mo−S bonds involving the coordinatively unsaturated S centers show little change from those involving bulk S atoms.

The results of the calculations for the slab thus provide a description of the electronic structure of both the 4-coordinate Mo sites on one side of the slab and the 2-coordinate S sites terminating the other side. Removal of the terminal S atoms from the $(10\bar{1}0)$ edge of MoS_2 leaves 4-coordinate Mo centers which are only slightly reduced relative to a bulk Mo center. At the same time, however, loss of two nearest-neighbor S atoms and two next-nearest-neighbor Mo atoms introduces a number of surface states in the region of the Fermi level. Most notably, a narrow Mo d_{yz} band is stabilized and partially filled. The doubly bridging S centers terminating the $(\bar{1}010)$ edge plane show a greater reduction than the surface Mo atoms on the opposite edge. The S levels are destabilized, relative to those of the bulk S atoms, and S *3p* lone pair electrons lead to the appearance of a new high energy occupied band. The strength of the Mo−S bonds involving the doubly bridging S atoms (S4) appears to be very similar to the strength of Mo−S bonds in the bulk.

Surface States of the 2-Coordinate Slab. Both surfaces of this slab also expose coordinatively unsaturated atoms: 2-coordinate Mo centers (Mo4 in Figure 3c) on one surface and terminal S atoms (S1 in Figure 3c) on the other surface. The total DOS for the slab, the projections of the surface Mo 4d orbitals, and the projections of the terminal S1 3s and 3p orbitals are plotted in Figure 5. Once again surface states arise from the unsaturated surface atoms, and the semiconducting gap observed in bulk MoS_2 is no longer observed. The partial (DOS) for the Mo d orbitals show that all of the Mo bands are affected by loss of the surface S atoms. The Mo d_{xz} band drops so much in energy that it is nearly filled. The d_{yz} band is also stabilized but remains unoccupied. In addition, the gap separating the bonding and antibonding combinations of the d_{z^2}, $d_{x^2-y^2}$, and d_{xy} orbitals disappears. The projection of the s and p bands of the terminal S atoms on the opposite side of the slab shows that these orbitals are destabilized even more than the orbitals of the bridging sulfurs on the 4-coordinate slab. A portion of the p band, which can now be associated with the presence of two lone pairs of electrons per S atom, is actually pushed up above the Fermi level and is thus unoccupied.

Calculated Mulliken charges, $F_{aa}{}^o$, and electrostatic potentials for all of the nonequivalent atoms are listed in Table 2. The exposed Mo atoms are highly coordinatively unsaturated, and it is not surprising that they are quite highly reduced. The Mo d orbitals are destabilized relative to both the bulk Mo atoms and the 4-coordinate Mo centers discussed above; the stabilizing effect of the loss of four negatively charged S atoms is not sufficient to offset the destabilizing effect of the increased Mo orbital occupations. As might be expected the Mo4−S4 overlap population indicates that the two remaining Mo−S bonds are stronger than those in the bulk. The Mo1−S1 overlap population indicates that the Mo−S bonds involving the terminal S atoms are also considerably strengthened over those in the bulk. The terminal S1 atoms carry a relatively low negative charge while Mo1 atoms carry a surprisingly high positive charge. The

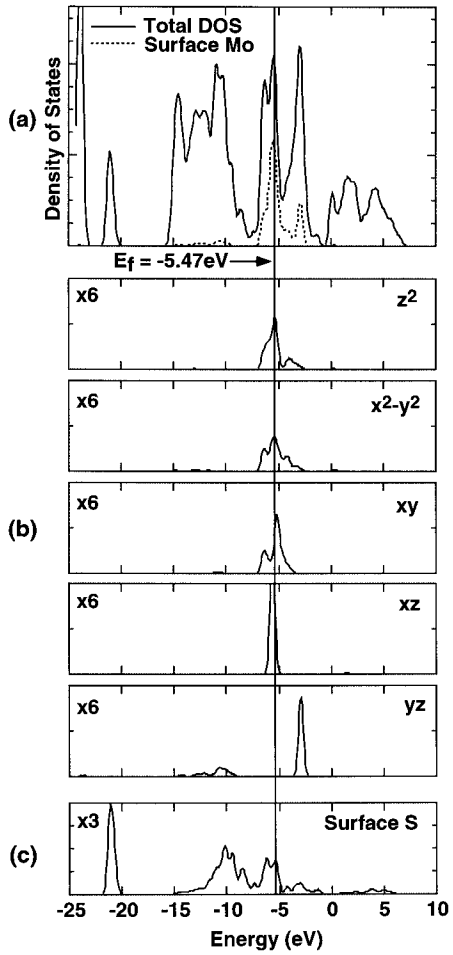

Figure 5. Calculated DOS for the MoS_2 slab exposing 2-coordinate Mo atoms. (a) Total DOS and projection of surface Mo (Mo4 in Figure 3c) orbitals. (b) Individual Mo4 4d orbital partial DOS. (c) Projection of surface S (S1 in Figure 3c) 3s and 3p orbital partical DOS.

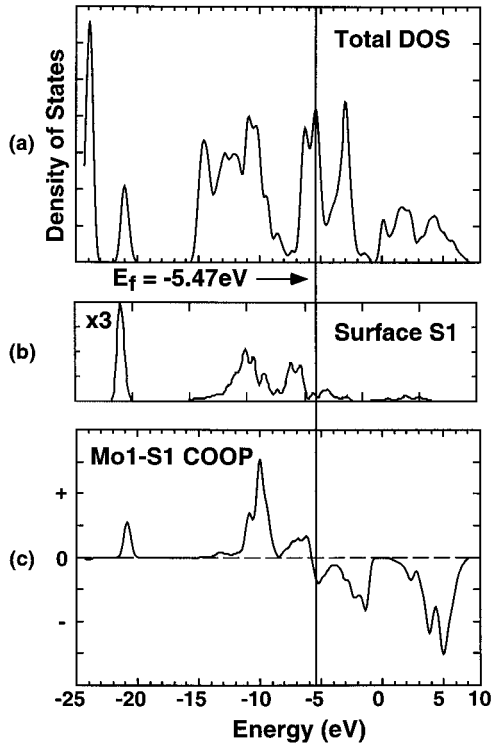

Figure 6. Calculated DOS and Mo1−S1 COOP for the MoS_2 slab exposing 2-coordinate Mo atoms. (a) Total DOS. (b) Projection of terminal S1 3s and 3p orbitals. (c) COOP between Mo1 and S1. (Mo1 and S1 are defined in Figure 3c.)

low negative charge on the terminal S atoms results from the incomplete filling of the destabilized p band associated with these atoms. The high positive charge on Mo1 comes about because, unlike the bulk Mo atoms, part of the Mo1 d_{z^2} band also lies above the Fermi level. The destabilization of part of both the terminal S p bands and the Mo1 d_{z^2} bands can be understood by considering the projections of the terminal S1 p orbitals, the projections of the Mo1 d orbitals, and the Mo1−S1 COOP curve (this COOP curve is shown in Figure 6). The COOP curve reveals that the sulfur p lone pair orbitals (between −5 and −7 eV) are not truly nonbonding but instead consist of components which are weakly bonding and weakly antibonding between the sulfur p orbitals and the Mo orbitals. These interactions involve primarily the Mo d_{z^2} orbital. Since the antibonding component, which is high in d_{z^2} character but also has S1 p character, is destabilized above the Fermi level, neither the Mo d_{z^2} nor the S1 "lone pair" bands are completely occupied. The Mo−S1 interactions thus increase the positive charge on Mo1, decrease the negative charge on S1, and strengthen the Mo1−S1 bond.

In summary, removal of bridging S atoms from the $(\bar{1}010)$ edge of MoS_2 leaves 2-coordinate Mo centers that are considerably reduced in comparison to bulk Mo centers. Loss of four nearest-neighbor S atoms and two next nearest-neighbor Mo atoms affects all of the Mo d bands and introduces a number of surface states in the area of the Fermi level. Notably, most of the narrow d_{yz} band actually lies below the Fermi level and is nearly completely occupied. Unexpectedly, the terminal S1 and the six-coordinate Mo1 on the fully sulfided edge are actually oxidized relative to the bulk atoms. The S levels are destabilized relative to the bulk S atoms, and weak interactions between the S lone pair orbitals (which lie particularly high in energy) and the Mo d_{z^2} orbital lead to a band having components that are both weakly bonding and weakly antibonding between Mo1 and S1. In contrast to bulk MoS_2, where the d_{z^2} band is fully occupied, part of this band is now more antibonding in character and is destabilized such that the band is only partially occupied. Since the band has both S and Mo character, both atoms show a loss of electron density. At the same time, however, the terminal Mo−S bonds are stronger than the Mo−S bonds in the bulk.

Decreasing the Dimensionality of MoS_2. All of the calculations discussed above take into account the three-dimensional layered structure of MoS_2. Because of this structure MoS_2 often grows in thin extended sheets, and discussions of catalytic activity often assume that MoS_2 exists as finite slabs of varying thickness.[9] It has been proposed that highly active MoS_2 may actually be a single-layer MoS_2 sheet, and previous extended Hückel calculations modeled MoS_2 by such a single-layer two-dimensional sheet.[29] A single layer MoS_2 sheet consists of just one of the MoS_2 layers shown in Figure 1a; it is periodic in the *x* and *y* directions but not in *z* because it is only one MoS_2 layer thick. If MoS_2 is modeled by such a sheet, the (100) edge planes can then be studied by slicing off a one-dimensional ribbon (rather than a two-dimensional slab). Use of such a ribbon greatly decreases the number of atoms which must be included in a unit cell for surface calculations. Because we wish to study more isolated S vacancies on these edges (necessitating a considerably larger unit cell in the *x* direction along the edge of a layer), it would be desirable to utilize a ribbon rather than a slab to model the edge planes. To first

Table 3. Calculated Mulliken Charges (q_A), Energy Levels (F_{aa}^o, eV, for Metal d and Sulfur p Orbitals), Potential Energies ($-Q_A$, EV), and Selected Mo−S Overlap Populations for a Single-Layer Sheet of MoS_2 and for the 4- and 2-Coordinate (100) Surface Ribbons

	q_A	F_{aa}^o	$-Q_A$
	MoS_2 Sheet		
Mo	1.21	−6.33	−9.61
S	−0.61	−11.34	6.85
	Mo−S overlap population 0.051		
	4-Coordinate Ribbon		
Mo1[a]	1.20[a]	−6.77	−8.63
Mo2	1.26	−7.00	−9.59
Mo3	1.21	−6.63	−9.29
Mo4	1.41	−6.56	−12.34
S1	−0.61	−11.84	7.32
S2	−0.57	−11.76	6.78
S3	−0.60	−11.54	6.95
S4[a]	−0.77	−9.43	6.85
	Mo4−S4 overlap population 0.089		
	2-Coordinate Ribbon		
Mo1	+1.37	−6.95	−11.41
Mo2	+1.211	−6.69	−9.21
Mo3	+1.26	−6.83	−9.84
Mo4[a]	+1.02	−6.15	−6.27
S1[a]	−0.64	−8.62	4.54
S2	−0.58	−11.69	6.94
S3	−0.58	−11.64	6.80
S4	−0.63	−11.63	7.35
	Mo1−S1 overlap population 0.131		

[a] Surface atoms as defined in Figure 3.

gauge the effects of removing the periodicity in the third dimension and to then determine whether a ribbon model is appropriate for further studies of the (100) edges, we performed calculations on several simplified MoS_2 systems. These include a two-dimensional single-layer MoS_2 sheet and two different ribbons exposing (100) edge plane atoms.

The DOS of the two-dimensional single-layer MoS_2 sheet is both qualitatively and quantitatively similar to the full bulk structure and is therefore not illustrated here. The calculated semiconducting gap (1.04 eV) is somewhat larger, however, than that calculated for the full three-dimensional structure (0.86 eV). The Mo and S atoms are calculated to be more positive and more negative, respectively (compare Tables 2 and 3), than in the three-dimensional bulk structure. This effect can be explained in terms of the removal of unfavorable repulsive interactions between the sulfur anions of neighboring basal planes. This results in decreased mixing of the Mo and S orbitals and increased occupation of the sulfur orbitals, i.e., a decrease in the covalency (or increase in the ionicity) of the molybdenum−sulfur bonding. The increased ionicity of the Mo−S bonds is also reflected in the Mo−S overlap population, which decreases from the bulk value of 0.081 to 0.051 in the two-dimensional sheet. A single-layer two-dimensional sheet of MoS_2 is therefore expected to be more ionic than the full three-dimensional structure. This result suggests that Mo−S bonds on a basal plane capping a "stack" of MoS_2 sheets should also show, although not as pronounced, an increase in ionicity.

The 4-coordinate and 2-coordinate ribbons were constructed in exactly the same manner as the 4-coordinate and 2-coordinate slabs described above and therefore can also be illustrated by Figure 3b and 3c. The illustrations now represent portions of ribbons rather than slabs since there is no translation in the *z* direction. The DOS curves of the ribbons are similar to those of the slabs and are not illustrated here. The calculated charges listed in Table 3 indicate that Mo−S bonding in the one-dimensional ribbons is also more ionic than in the 4- and 2-coordinate slabs. Comparisons between the values listed in Tables 2 and 3 illustrate, however, that the differences between surface and bulk atoms show consistent trends in going either from bulk MoS_2 to a surface slab or from a sheet of MoS_2 to a surface ribbon. Interestingly, however, the Mo−S bonds along the fully sulfided edge of each ribbon (Mo4−S4 in Figure 3b and Mo1−S1 in Figure 3c) appear to be stronger than the corresponding bonds in the two-dimensional slabs. This comes about primarily because of the absence of an adjacent MoS_2 layer. In the calculations on the two-dimensional slabs, the alternating pattern of the MoS_2 layers in the slabs allows the edge S atoms of each layer to feel the stabilizing effect of the coordinatively unsaturated Mo atoms on the edges of adjacent layers. Removal of these adjacent layers destabilizes the energy levels on the edge S atoms; this in turn strengthens the Mo−S edge bonds. While this effect is to some degree an artifact of the structures of the slabs and ribbons used for the calculations, it illustrates that the strengths of the edge Mo−S bonds appear to be sensitive not only to the presence of adjacent layers but also to the way in which the adjacent layers are terminated.

Although the Mo−S bonding in both the MoS_2 sheet and the one-dimensional ribbons is more ionic than in bulk MoS_2 or in the two-dimensional slabs, the differences between bulk and surface atoms show consistent trends in the two systems. This suggests that the ribbons can serve as the bases for further studies of more isolated S vacancy patterns. The reduction in dimensionality from slabs to ribbons greatly reduces the size of the unit cell needed for these studies, and we will make use of the one-dimensional ribbons for further studies of MoS_2 edges.

Conclusions

The results presented here verify that the Fenske−Hall method provides a reliable description of the electronic structure of inorganic solids containing transition metals. These results, as well the results of test calculations for a number of other inorganic solids, suggest that this method will be particularly useful for examining the electronic structure of the surfaces of catalytic materials such as transition metal sulfides and oxides.

The calculated electronic structure of bulk MoS_2 is in reasonable agreement with previous experimental and theoretical studies and provides the basis for studies of surface electronic structure. Results of calculations for MoS_2 slabs exposing 4- and 2-coordinate Mo atoms and bridging and terminal S atoms provide a description of coordinatively unsaturated edge atoms. Four-coordinate Mo atoms are only slightly reduced relative to bulk Mo atoms, while the reduction is much more pronounced for 2-coordinate Mo atoms. Coordinative unsaturation of the Mo atom introduces surface states near the Fermi level, and, not surprisingly, this effect is more pronounced for the 2-coordinate Mo atoms. Comparisons of bulk and surface Mo−S overlap populations indicate that while surface Mo−S bonds involving bridging S atoms are comparable in strength to bulk Mo−S bonds, surface Mo−S bonds which involve terminal S atoms are considerably stronger than bulk Mo−S bonds. This suggests that removal of terminal S atoms to form coordinatively unsaturated Mo sites may be more difficult than removal of bridging S atoms.

The results of calculations for a single-layer two-dimensional sheet of MoS_2 show that the bonding in a single layer of MoS_2 is more ionic than in bulk MoS_2. While this same effect is observed in one-dimensional surface ribbons, consistent changes

between bulk and surface electronic structure are observed in comparisons between bulk MoS_2 and surface slabs and between a sheet of MoS_2 and one-dimensional surface ribbons. This indicates that one-dimensional ribbons can be used to study different types of surface sites for MoS_2, and we are making use of the ribbons to study other types of coordinatively unsaturated Mo atoms, different S-vacancy patterns, and possible models for Co or Ni promoted edge planes.

The results presented here are part of a larger study of HDS catalysis. We are particularly interested in understanding how the electronic structures of transition metal sulfides are related to their activity as HDS catalysts, and we are carrying out a systematic study of the bulk and surface electronic structure of metal sulfides which can act as HDS catalysts. Two sulfides that exhibit high HDS activity are RuS_2 and Rh_2S_3, and results of Fenske−Hall band structure calculations for these two materials are described in another paper.[27]

Acknowledgment. Support of this work through National Science Foundation Grant CHE94-21784 is gratefully acknowledged. A.T. also thanks NSF EPSCoR for support.

Appendix: The Ewald Method of Evaluating Electrostatic Potentials

The problem at hand is the evaluation of the electrostatic potential at a center A in the zeroth unit cell:

$$-Q_A = \sum_\tau \sum_{C \neq A^o} \frac{q_C}{R_{AC}{}^\tau} \tag{A1}$$

where C includes A in other unit cells but not the zeroth. This sum is conditionally convergent, and its evaluation is greatly facilitated by the use of standard techniques such as the Ewald method.[31−33]

In the Ewald method, the charge distribution is divided into two components. At an arbitrary point $\vec{r}$ these are

$$\rho_1(\vec{r}) = \sum_\tau \sum_C q_C \left[\delta(\vec{r}_C{}^\tau - \vec{r}) - \frac{\eta^3}{\pi^{3/2}} e^{-\eta^2(\vec{r}_C{}^\tau - \vec{r}^2)} \right]$$

$$\rho_2(\vec{r}) = \sum_C q_C \left[\sum_\tau \frac{\eta^3}{\pi^{3/2}} e^{-\eta^2(\vec{r}_C{}^\tau - \vec{r})} - \frac{1}{v} \right] \tag{A2}$$

where v is the volume of the unit cell. The potential $V_1(\vec{r})$ due to the first component is readily evaluated:

$$V_1(\vec{r}) = \sum_\tau \sum_C q_C \left[\frac{\mathrm{erfc}(\eta |\vec{r}_C{}^\tau - \vec{r}|)}{|\vec{r}_C{}^\tau - \vec{r}|} + \text{constant} \right] \tag{A3}$$

If the unit cell is electrically neutral, the constant term cancels out.

The second component of the charge distribution is expressed as a Fourier series. This is straightforward for a three-dimensional lattice:

$$\rho_2(\vec{r}) = \frac{1}{v} \sum_C \sum_{k \neq 0} q_C e^{-k^2/4\eta^2} e^{i\vec{k}\cdot(\vec{r}_C - \vec{r})} \tag{A4}$$

where $\vec{k}$ is a reciprocal lattice vector. The potential is obtained by solving Poisson's equation

$$\nabla^2 V = -4\pi\rho \tag{A5}$$

which yields

$$V_2(\vec{r}) = \frac{4\pi}{v} \sum_C \sum_{k \neq 0} q_C \frac{1}{k^2} e^{-k^2/4\eta^2} e^{i\vec{k}\cdot(\vec{r}_C - \vec{r})} \tag{A6}$$

Since

$$-Q_A = V_1(\vec{r}_A) + V_2(\vec{r}_A) - \frac{2\eta}{\sqrt{\pi}} q_A \tag{A7}$$

where the correction $2\eta q_A/\pi^{1/2}$ takes into account that the potential due to the charge distribution at A must be omitted, we have

$$-Q_A = \sum_{C \neq A^o} q_C \left\{ \frac{4\pi}{v} \sum_{k \neq 0} \frac{1}{k^2} e^{-k^2/4\eta^2} e^{i\vec{k}\cdot(\vec{r}_C - \vec{r}_A)} + \sum_\tau \frac{\mathrm{erfc}(\eta R_{AC}{}^\tau)}{R_{AC}{}^\tau} \right\} - \frac{2\eta}{\sqrt{\pi}} q_A \tag{A8}$$

The parameter η is chosen to maximize convergence; we have found $\eta = 0.2$ to be a suitable value.

For a lattice which is periodic in two dimensions, $V_1(\vec{r})$ assumes the same form as in eq A3. The evaluation of $V_2(\vec{r})$ is somewhat more involved. One way of dealing with it is to begin with the expression in eq A6 and recognize that the summation over k space in the nonperiodic dimension needs to be replaced by a Fourier integral. This integral can be solved analytically, and gives[34]

$$V_2(\vec{r}) = \frac{\pi}{a} \sum_{k \neq 0} \sum_C q_C \frac{1}{k} e^{i\vec{k}\cdot\vec{r}_\parallel} \left[e^{kr_\perp} \mathrm{erfc}\left(\frac{k}{2\eta} + \eta r_\perp \right) + e^{-kr_\perp} \mathrm{erfc}\left(\frac{k}{2\eta} - \eta r_\perp \right) \right] \tag{A9}$$

Here a refers to the area of the unit cell; $\vec{r}_\parallel$ and $\vec{r}_\perp$ are the projections of the vector distance $(\vec{r}_C - \vec{r})$ parallel and perpendicular to the plane of periodicity, respectively; and the k space summation is in two dimensions.

The other way is to expand $\rho_2(\vec{r})$ as a Fourier series in two dimensions:

$$\rho_2(\vec{r}) = \frac{\eta}{a\sqrt{\pi}} \sum_{k \neq 0} \sum_C q_C e^{-\eta^2 r_\perp{}^2} e^{-k^2/4\eta^2} e^{i\vec{k}\cdot\vec{r}_\parallel} \tag{A10}$$

and then solve the two-dimensional Poisson equation

$$\nabla^2 V = -2\pi\rho \tag{A11}$$

This yields

(31) Tosi, M. P. *Solid State Physics* **1964**, *16*, 1.
(32) de Leeuw, S. W.; Perram, J. W.; Smith, E. R. *Roc. R. Soc. London* **1980**, *A373*, 27.
(33) Heyes, D. M. *J. Chem. Phys.* **1981**, *74*, 1924.
(34) Parry, D. E. *Surf. Science* **1975**, *49*, 433.

$$V_2(\vec{r}) = \frac{2\eta\sqrt{\pi}}{a}\sum_{k\neq 0}\sum_{\mathrm{C}} q_{\mathrm{C}}\, \mathrm{e}^{-\eta^2 r_\perp{}^2}\frac{1}{k^2}\mathrm{e}^{-k^2/4\eta^2}\mathrm{e}^{i\vec{k}\cdot\vec{r}_{\parallel}} \quad \text{(A12)}$$

A similar procedure as in eqs A10−A12 was apparently invoked to calculate a modified electrostatic sum in a periodic MINDO formalism.[35]

It turns out that for a "flat" lattice, i.e. with all $r_\perp = 0$, eqs A9 and A12 yield identical results. (For a two-dimensional centered NaCl lattice with a nearest-neighbor separation of 2.814 Å, the Madelung constant, which is $2.814|Q_{\mathrm{Na}}|$, was calculated to be 1.616, as compared to 1.748 for a 3-D lattice.) For a slab of finite thickness, however, eq A12 yields reasonable potential energies, while eq A9 appears to do rather poorly. (While the source of the error in eq A9 is not entirely clear, the $\mathrm{e}^{kr_\perp}$ term in eq A9 may cause divergence.) We have therefore made use of eq A12 when the lattice is periodic in two dimensions.

Using a similar procedure for a one-dimensional lattice, where the Poisson equation is now $\nabla^2 V = -\rho$, one obtains

$$V_2(\vec{r}) = \frac{\eta^2}{\pi l}\sum_{k\neq 0}\sum_{\mathrm{C}} q_{\mathrm{C}}\, \mathrm{e}^{-\eta^2 r_\perp{}^2}\frac{1}{k^2}\mathrm{e}^{-k^2/4\eta^2}\mathrm{e}^{i\vec{k}\cdot\vec{r}_{\parallel}} \quad \text{(A13)}$$

where l is the length of the unit cell. Once again, the potential energies obtained are physically reasonable. As an example, the Madelung constant for one-dimensional NaCl was calculated to be 1.386, which compares well with a brute force calculation.

(35) Craig, B. I.; Smith, P. V. *Surf. Science* **1989**, *210*, 468.

IC970874V